Magnetic phase diagram of the antiferromagnetic cobalt tellurate Co_3TeO_6

J. L. Her,[1,2] C. C. Chou,[3] Y. H. Matsuda,[2,*] K. Kindo,[2] H. Berger,[4] K. F. Tseng,[3] C. W. Wang,[5] W. H. Li,[5] and H. D. Yang[3,†]

[1]*Division of Natural Science, Center for General Education, Chang Gung University, Tao-Yuan 333, Taiwan*

[2]*Institute for Solid State Physics, The University of Tokyo, Kashiwa, Chiba 277-8581, Japan*

[3]*Department of Physics, National Sun Yat-Sen University, Kaohsiung 804, Taiwan*

[4]*Institutes of Physics of Complex Matter, EPFL, Lausanne, Switzerland*

[5]*Department of Physics, National Central University, Chung-Li 32001, Taiwan*

(Received 1 September 2011; revised manuscript received 5 December 2011; published 16 December 2011)

In this study, we measured the temperature-dependent magnetic susceptibility [$\chi(T)$], ac magnetic susceptibility [$\chi_{ac}(T)$], specific heat [$C_p(T)$], and high-field magnetization [$M(H)$] of a newly synthesized single-crystalline material, Co_3TeO_6. Two transitions were observed in $\chi(T)$ and $C_p(T)$ curves at values of T_{N1} and T_{N2} of approximately 26 and 18 K ($H = 0$), respectively. The high-field $M(H)$ curves exhibited strong magnetic anisotropy and several field-induced transitions, suggesting that the magnetic ground state was complicated. Large spin-lattice coupling was evident by the large hysteresis in the $M(H)$ curves and through analysis of the specific heat data. We propose herein an H-T phase diagram that is consistent with our experimental findings.

DOI: 10.1103/PhysRevB.84.235123 PACS number(s): 75.30.Kz, 75.40.Cx, 75.50.Ee, 75.60.Ej

I. INTRODUCTION

Transition metal tellurides comprise a family of compounds that have a variety of physical properties and exhibit coupling between their spin, charge, and lattice phenomena. Tellurium ions play important roles in these compounds.[1–3] For example, in the two-dimensional (2D) spin system, $Ni_5(TeO_3)_4X_2$ (X = Br and Cl), the lone pair electrons in Te^{4+} cations serve as good separators between the 2D layers as a result of Coulombic repulsive force.[1] In $FeTe_2O_5Br$, which exhibits multiferroic phenomena, the lone pair electrons are polarized at the magnetic ordering temperature.[2] Very recently, Ni_3TeO_6 was suggested as a potential candidate for multiferroic properties because of its noncentrosymmetric crystal structure and the anisotropy of its magnetic moments. Neutron diffraction data has revealed, however, that the low-temperature spin structure of Ni_3TeO_6 is a collinear antiferromagnetic (AFM) with ferromagnetic(FM) honeycomb planes and no electric polarization was observed.[3]

Co_3TeO_6 is a newly synthesized compound that belongs to the family of transition-metal tellurides. Its crystal structure is the same as β-Li_3MF_6 (M = V, Cr, and Ti) with the monoclinic space group $C2/c$.[4] The Co^{2+} ions, which serves as the magnetic centers, are located in five crystallographically distinct sites (i.e., one tetrahedral and four octahedral sites) and connected by corner-, edge-, and face-sharing through Co-O bonds. Unlike the isostructural β-Li_3MF_6 compounds, where the interactions between the magnetic ions are small, the exchange interactions between the Co^{2+} ions in Co_3TeO_6 are sufficiently strong to result in long-range magnetic ordering.[4–6] Due to the crystal-field effect, the $3d$ electrons of the Co^{2+} ions have different configurations in the tetrahedral and octahedral sites. A well-known analog is spinel $Co^{2+}Co_2^{3+}O_4$, which possesses spatial inhomogeneity of its magnetic moment.[7] Because the structure of Co_3TeO_6 has features similar to those of spinel compounds, its low-temperature magnetic properties of Co_3TeO_6 are likely to be very interesting. In addition, the structures and phase transitions of A_3TeO_6 (A = Mn, Co, and Ni) have recently been studied, with dielectric measurement above room temperature.[8] The authors suggested that A_3TeO_6 compounds and their solid solutions are possible new multiferroics. Very recently, M. Hudl *et al.* showed that this compound behaves magnetic-field-driven electric polarization at low temperatures, indicating the existence of strong coupling between magnetic and electric dipoles.[9] No mater, A_3TeOF_6 compounds are multiferroic materials or not, the magnetic property is very important and is the base of studying the magnetodielectric coupling.

To understand the magnetic properties of Co_3TeO_6 at low temperature, in this study we focused on measuring its field-dependent magnetization and specific heat. The high-field magnetization processes exhibited several field-induced spin-flop transitions in pulsed magnetic fields up to 55 T. We observed large hysteresis of the field-induced transitions, suggesting that spin-lattice coupling would be large in Co_3TeO_6.

II. EXPERIMENTS

Through chemical vapour transport redox reactions in sealed evacuated silica tubes, Co_3O_4 (Alfa Aesar 99.7%), TeO_2 (Acros 99%), and $CoCl_2$ (Alfa Aesar 99.9%) were mixed in the off-stoichiometric molar ratio 4 : 3 : 1 and then were placed in a two-zone furnace with charge- and growth-zone temperatures of 973 and 873 K, respectively.[4] Needlelike dark-violet single-crystal samples, with a typical size of $2 \times 1 \times 1$ mm, were characterized by Oxford Xcalibur diffractometer, showing space group $C2/c$ (ICSD code: 249133) (see Fig. 1). The ceramic powder samples were prepared from the high purity $Co(NO_3)\cdot 6H_2O$ and telluric acid H_2TeO_4 with proper weight ratio. The mixtures were calcined at 770 K for 7 hours and then annealed at 970 K after they were grounded and pressed. The ceramic powder samples were characterized by D5000 (Siemens) x-ray powder diffractometer, and patterns are in good fit to group $C2/c$. Most of measurements were performed on the single crystal. The ceramic powder samples were only used in ac susceptibility measurements. Temperature-dependent magnetization was measured using

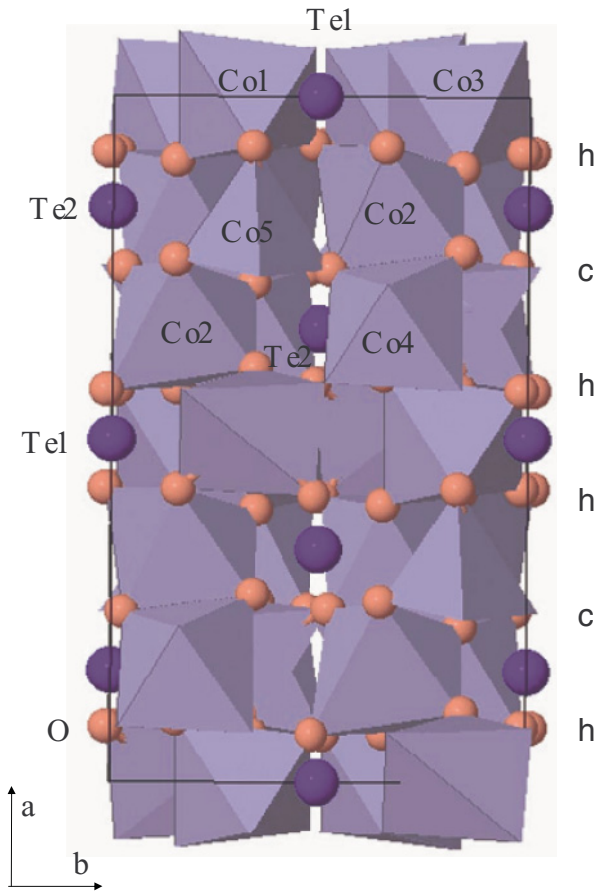

FIG. 1. (Color online) The structure of Co_3TeO_6 with two TeO_6 octahedra, four CoO_6 octahedra, and one CoO_4 tetrahedra in a mixed hexagonal-cubic hhchhc six layer.[4] The smaller sphere is O.

the SQUID magnetometer (Quantum Design MPMS) in the temperature range of 2–300 K under a 70 kOe field. The magnetic field was applied along the a and c crystalline axes. The high-field magnetization $M(H)$ was measured using an induction method with a pulse magnet. This system could generate pulse fields of up to 55 T with a duration time of 40 ms. The as-measured high-field magnetization behavior is similar to that measured by low-field technique, such as SQUID magnetometer. Therefore the obtained data were usually calibrated by multiplying certain factor. The factors were determined by comparing the low-field part curves of high- and low-field magnetization measurements. We carefully calibrated the high-field magnetization curves through low-field magnetization measurements, which were also performed using the SQUID magnetometer. The field-dependent specific heat was measured using a physical properties measurement system (Quantum Design PPMS). To ignore the effect of the thermal contact between the sample and the holder, the specific heat was measured along only the $H\|a$-axis configuration.

III. RESULTS

A. Magnetic susceptibility

Figure 2(a) displays the temperature-dependent magnetic susceptibility data as well as the inverse magnetic susceptibility and the Curie-Weiss fitting results. We observe

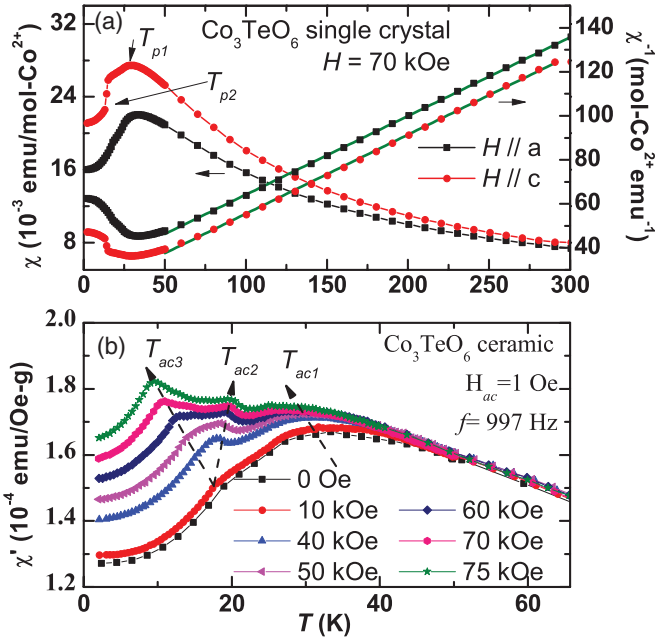

FIG. 2. (Color online) (a) Left axis: χ-T curves, right axis: χ^{-1}-T curves; green solid lines: curves fitted by using the Curie-Weiss law. (b) The ac susceptibilities under several selected dc fields.

several interesting features. First, the absolute value of the susceptibility along the $H\|a$ axis $[\chi_c(T)]$ is larger than that along the $H\|a$ axis $[\chi_a(T)]$ in the measured temperature range, indicating that an anisotropic effect occurs even at high temperatures. Second, in the $\chi_a(T)$ curves, an obvious peak (T_{p1}) appears at approximately 34 K with a barely observable shoulder (T_{p2}) at ~19 K. In the $\chi_c(T)$ curves, however, the main peak (T_{p1}) had shifted to ~29 K, accompanied by a sudden drop in susceptibility for T_{p2} at ~14 K. The peaks' positions and shapes were orientation dependent.

We fitted the high-temperature portion of the $\chi(T)^{-1}$ curves ($T > 50$ K) to the Curie-Weiss law

$$\frac{1}{\chi} = \frac{T - \Theta}{C}, \tag{1}$$

where Θ is the paramagnetic Curie temperature and C is the Curie-Weiss constant. By using the equation, $C = N\mu_{\text{eff}}^2/3k_B$, we obtained paramagnetic effective moments of 4.74 and 4.73 μ_B/Co^{2+} in the $H\|a$- and c-axis configurations, respectively. The effective moment of Co^{2+} ions is greater than the spin-only value, saying $\mu_{\text{eff}} = 3.88$ μ_B/Co^{2+}, and suggesting that the spin-orbital coupling contributes to the magnetic moment. The transition temperatures and the fitted parameters as well as effective moments are listed in Table I. The value of μ_{eff} that we obtained is very close to that of the six-coordinated Co^{2+} ions in Co_3O_4 (4.74 μ_B/Co^{2+}) and four-coordinated Co^{2+} ions of theoretical calculation (4.4 μ_B/Co^{2+}).[7,10] The negative Curie-Weiss temperatures indicate antiferromagnetic exchange interactions between the Co^{2+} ions. It should be noted that the μ_{eff} values are nearly identical, indicating that the anisotropic behaviors are significant near the transition temperatures.

TABLE I. Transition temperatures and Curie-Weiss law fitting results.

	$\chi(T)$		Curie-Weiss fit			$C_p(T)$[in zero field]	
Field direction	$T_{p1}(K)$	$T_{p2}(K)$	Θ (K)	C (emu/mol-Co^{2+})	μ_{eff} (μ_B/Co^{2+})	T_{N1} (K)	T_{N2} (K)
a axis	34	19	−79.5	2.80	4.74	26	16
c axis	29	14	−54.5	2.78	4.73	...	...

B. Specific heat

As mentioned above, the transition temperatures in the $\chi_a(T)$ and $\chi_c(T)$ curves are different because of the anisotropy. A better approach for determining the transition temperatures is to measure the specific heat under zero field. The solid line in Fig. 3(a) represents the temperature-dependent specific heat curve in the temperature range of 2.5–300 K. The as-measured specific heat, $C_p(T)$, includes the contributions from the magnetic ordering and the structural phase transition [$C_m(T)$], as well as the lattice vibration [$C_L(T)$]. To remove the contribution from the thermal fluctuation of lattice, we used the Debye model to fit the specific heat data:

$$C_L = 9Rx_D^{-3}\int_0^{x_D}\frac{x^4e^x}{(e^x-1)^2}dx, \tag{2}$$

where $x_D = \Theta_D/T$, Θ_D is the Debye temperature, and R is the molar gas constant [8.31 J/(mole K)]. The value of $C_m(T)$ can, therefore, be obtained using the equation $C_m(T) = C_p(T) - C_L(T)$. Figure 3(a) presents the resulting low-temperature $C_m(T)$ data as a red dotted line.

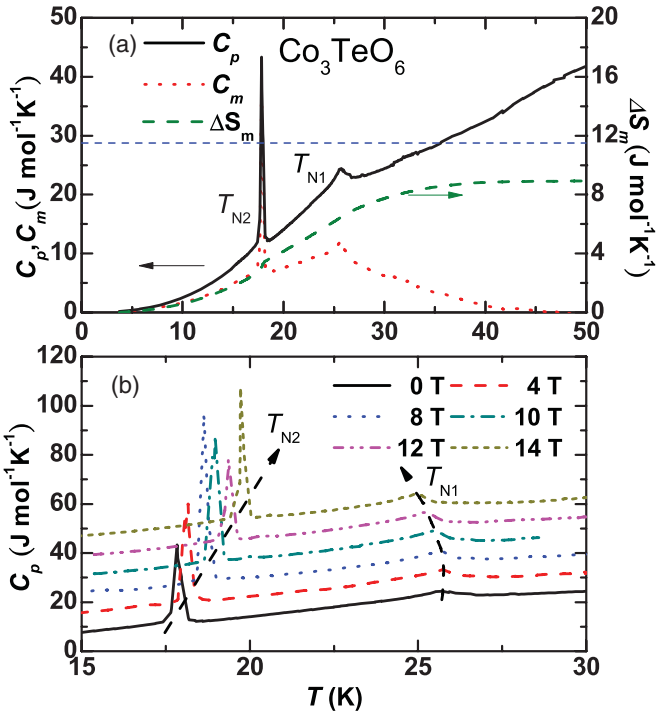

FIG. 3. (Color online) (a) Black solid line: $C_p(T)$ in zero field; red dot line: $C_m(T)$; green dashed line; entropy change; horizontal blue dash line: expected magnetic entropy change of an $S = 3/2$ spin system. (b) $C_p(T)$ curves measured under different magnetic fields ($H \| a$ axis). The curves are stacked by an offset of 8 J/(mole K).

At a temperature of approximately 26 K (T_{N1}), we observed a λ-shaped transition peak, which should correspond to T_{p1}, suggestive of a long-range magnetic ordering (LRMO) transition. In the lower-temperature region, another sharp spikelike anomaly ($T_{N2} \sim 18$ K) was present, inferring another transition. Because the zero-field specific heat measurement was independent of sample orientation, the observation of two anomalies indicates only two transitions in this temperature region. In addition, there is the presence of a broad background, which started at approximately 40 K, suggested that a short-range magnetic ordering (SRMO) appeared up at approximately 40 K. This result is consistent with that from a previous report, in which the specific heat was measured for a ceramic sample.[8]

Usually, the transition between magnetic ordering phases does not cause a large change in entropy, resulting in the absence of peak in the specific heat data. The spikelike peak is more likely to correspond to a change in another degree of freedom, namely, a lattice structural phase transition. The presence of T_{N2} in the specific heat measurement and T_{p2} in the $\chi(T)$ curves suggests that there is a strong coupling between spin and lattice degree of freedom.

We calculated the entropy change using the equation

$$\Delta S_m(T) = \int_0^T \frac{C_m(T)}{T}dT. \tag{3}$$

The values of $\Delta S_m(T)$ are also presented in Fig. 3(a). A small jump in the value of $\Delta S_m(T)$ appears at 18 K, which represents the contribution of the spikelike anomaly T_{N2}. The measured total ΔS_m is ~8.9 J/(mole K). This value is lower than the magnetic entropy change for an $S = 3/2$ spin system, where $\Delta S_m(T)$ is equal to $R\ln(2S+1)$ and has a value of 11.5 J/(mole K), presumably because of the difficulty in fitting the $C_L(T)$ curve precisely.

Figure 3(b) presents the specific heat curves plotted as a function of the magnetic field ($H \| a$ axis); they provide a better idea of the nature of the two transitions. On one hand, we observe that T_{N1} shifted toward lower temperatures upon increasing the magnetic field, which is a typical behavior of an AFM-like ordering. On the other hand, T_{N2} shifted toward higher temperatures, which represents the FM-like tendency. Therefore the observation of the magnetic field dependence of T_{N2} peak indicates that there are degrees of freedom closely coupling with the spins.

We observed similar field dependence in ac susceptibility $\chi_{ac}(T)$ curves. Figure 2(b) presents the dc field-dependent $\chi_{ac}(T)$ curves that we measured using a ceramic sample. Under zero field, a broad peak (T_{ac1}) and a small hump were evident at approximately 30 and 18 K, respectively, consistent with the dc magnetization data. The small hump, corresponding to T_{N2}, became more obvious and split into

two peaks under higher fields; again, the higher- (T_{ac2}) and lower-temperature (T_{ac3}) signals exhibited FM- and AFM-like tendencies, respectively. This behavior was probably due to the mixing of the orientations in the ceramic sample, with the T_{ac2} (T_{ac3}) signal related to the microcrystals having the weak FM component parallel (perpendicular) to the magnetic field. The coexistence of FM- and AFM-like behaviors suggests that the ground state is not a pure or typical AFM but a canted AFM or the other complex spin structure.

C. High-field magnetization

Figure 4 displays high-field magnetization process curves that we recorded at selected temperatures. In Fig. 4(a), the curves were measured with the magnetic field orientated to the a axis. A clear jump in the magnetization occurred with a value of H_{a1} of approximately 17 T at the lowest temperature studied (2.2 K). The variation of magnetization in $H \| b$ axis is very similar to $H \| a$ axis and is not shown for clarity. In addition, magnetic hysteresis is evident in the descending-field process. This jump usually arises from the field-induced reorientation of the easy axis, which induces the spins to undergo a spin-flop transition. In addition, the magnetic moment under the 55 T field at 2.2 K, was only 1.79 μ_B/Co^{2+}. This value is much less than the expected fully aligned saturated moment of approximately 3 μ_B/Co^{2+} (considering spin only). In the absence of any other field-induced transition under higher fields, we would estimate the saturated moment to be reached at approximately 110 T.

In Fig. 4(b), recorded with $H \| c$ axis, we observe two field-induced phase transitions at values of H_{c1} and H_{c2} of approximately 12 and 26 T, respectively, at 2.5 K. The opened hysteresis loops having magnetic field widths, 4.5 and 2 T near H_{c1} and H_{c2}, respectively, is even larger than those in Fig. 4(a). Large hysteresis may originate from the coupling between spin and lattice. Upon increasing the temperature, all of the hysteresis loops decreased in size, eventually becoming unobservable. Moreover, as the temperature increased, the value of H_{c2} became nearly temperature independent; in contrast, H_{c1} shifted toward lower field and disappeared into the curve recorded at 20 K. This behavior suggests that a critical temperature exists between 15 and 20 K, which is close to T_{N2}. Similarly, the magnetic moment at the lowest temperature and highest field was ~2.1 μ_B/Co^{2+}, still less than the fully aligned saturated moment.

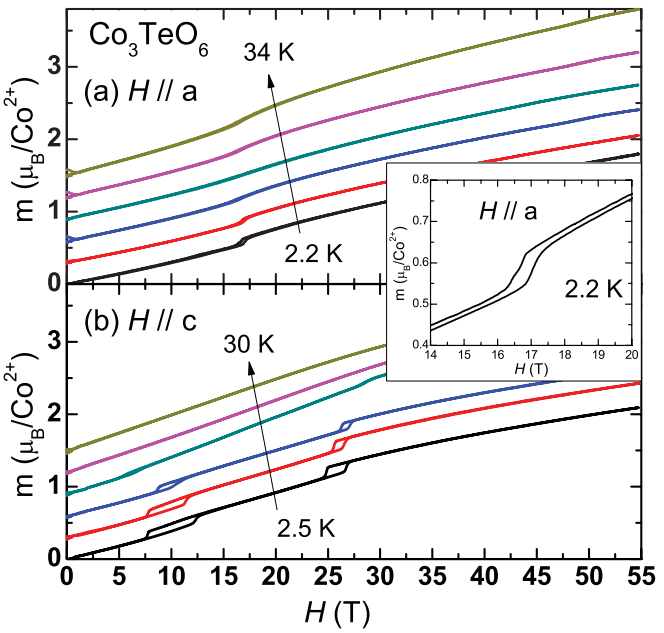

FIG. 4. (Color online) High-field magnetization process curves measured at several selected temperatures: (a) $H \| a$ axis at 2.2, 4.2, 10, 15, 20, and 34 K; and (b) $H \| c$ axis at 2.5, 4.2, 10, 15, 20, and 30 K. The curves are stacked by an offset of 0.3 μ_B/Co^{2+}. The inset is the enlarged part of magnetization with $H \| a$ axis at 2.2 K around 17 T.

IV. DISCUSSIONS

Figure 5 is an H-T phase diagram of Co_3TeO_6 with $H \| c$; it summarizes the results described in previous paragraphs. First, SRMO began to appear at a temperature below 40 K. When the sample was cooled down to T_{N1}, the spins of Co^{2+} ions began to exhibit an AFM ordering, as supported by the magnetization and specific heat data. When we further lowered the temperature to T_{N2}, a lattice-distorted change occurred. Almost at the same temperature, the spins underwent a spin reorientation transition. As a result, we observed a sudden drop in $\chi_c(T)$ and a small hump in $\chi_a(T)$.

The presence of multistep spin-flop transitions in the high-field magnetization processes suggests that the magnetic ground state of Co_3TeO_6 might be a super-AFM phase, similar to those of $Ni_5(TeO_3)_4X_2$ (X = Br and Cl) compounds.[1,2,11–13] In this case, there are several pairs of antiparallel spin sublattices, where competition between the Zeeman energy and the complex anisotropic energies of the different Co^{2+} ions leads to many spin-flop transitions during the high-field

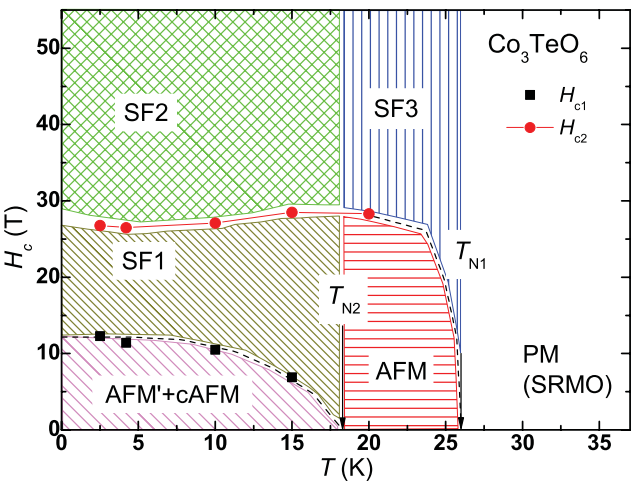

FIG. 5. (Color online) H-T phase diagram of Co_3TeO_6. The phase boundary is determined from the zero-field specific heat and high-field magnetization ($H \| c$ axis) results. The dashed lines crossing to temperature axis at T_{N1} and T_{N2} are merely guides for the eyes. PM(SRMO): Paramagnetic state with short-range magnetic ordering; AFM and AFM′: antiferromagnetic states; cAFM: canted antiferromagnetic state. SF1, SF2, and SF3: field-induced spin-flopped states.

magnetization process. Notably, the T_{N2} transition has an FM-like tendency in the field-dependent specific heat curves, indicating that at least one pair of the antiparallel spin sublattices is slightly canted to give a weak ferromagnetic component. In Fig. 5, we denote this phase as (AFM′ + cAFM). Low-temperature AFM′ phase is probably different with AFM phase. The canted-type magnetic order state is one possible spin state that can exhibit a magnetocapacity effect.[14] In the absence of a low-temperature crystal structure, we cannot know whether the crystal loses its centrosymmetry at low temperature. The canted-type magnetic ordering and large spin-lattice coupling do, however, support the notion that Co_3TeO_6 might be a multiferroic compound at $T < T_{N2}$.

In addition to AFM and cAFM, other spin structures are also possible at low temperature, due to the complicated crystal structure and exchange pathways. For example, the spin density wave is also a candidate state that does not conflict with antiferromagnetic exchange interactions. One hint arises from the specific heat data. The specific heat near T_{N1} provided a mean-field-like increase, with a value of $\Delta C/T_{N1}$ of approximately 1.53 J/(mole K). Compared with the usual BCS expression of SDW ($\Delta C/T_{\mathrm{SDW}} = 1.4\gamma$), we obtain a value of γ of approximately 4 mJ/(mole K). This value is close to, but slightly smaller than, that [5 mJ/(mole K)] for the organic SDW material $(TMTSF)_2PF_6$.[15] Additional studies, such as temperature- and magnetic-dependent x ray and neutron diffraction, may provide evidences and help to clarify the spin structure and spin-lattice effects mentioned above.

V. SUMMARY

Co_3TeO_6 undergoes two phase transitions upon decreasing the temperature. At temperatures between 18 and 26 K, this compound formed an AFM phase; it transformed into an AFM′ + cAFM phase at temperatures below 18 K, as revealed in plots of $C_p(T)$ and in high-field $M(H)$ data. In addition, high-field $M(H)$ curves featured large hysteresis at temperatures below 18 K, suggesting that the spin-lattice coupling was strong in the low-temperature phase. Our results confirm that the low-temperature phases are complex, with other spin structures (e.g., SDW) possibly existing.

ACKNOWLEDGMENTS

This study was supported by the National Science Council of Taiwan, R.O.C. under Grant Nos. NSC 99-2112-M-182-001-MY2 and NSC 100-2112-M-110-004-MY3.

*Also at PRESTO, Japan Science and Technology Agency, Saitama, Saitama 332-0012.

†Corresponding author: yang@mail.phys.nsysu.edu.tw

[1] M. Johnsson, K. W. Tornroos, P. Lemmens, and P. Millet, Chem. Mater. **15**, 68 (2003).

[2] M. Pregelj, O. Zaharko, A. Zorko, Z. Kutnjak, P. Jeglič, P. J. Brown, M. Jagodič, Z. Jagličič, H. Berger, and D. Arčon, Phys. Rev. Lett. **103**, 147202 (2009).

[3] I. Živković, K. Prša, O. Zaharko, and H. Berger, J. Phys. Condens. Matter **22**, 056002 (2010).

[4] R. Becker, M. Johnsson, and H. Berger, Acta Crystallogr. **C62**, i67 (2006).

[5] A. K. Tyagi, R. Pottgen, and J. Kohler, Z. anorg. allg. Chem. **622**, 1329 (1996).

[6] A. Tyagi and J. KoNhler, Mater. Res. Bull. **35**, 135 (2000).

[7] Y. Ikedo, J. Sugiyama, H. Nozaki, H. Itahara, J. H. Brewer, E. J. Ansaldo, G. D. Morris, D. Andreica, and A. Amato, Phys. Rev. B **75**, 054424 (2007).

[8] N. Golubko, V. Proidakova, G. Kaleva, S. Ivanov, A. Mosunov, S. Stefanovich, N. Sadovskaya, E. Politova, and P. Nordblad, Bull. Russ. Acad. Sci. Phys. **74**, 724 (2010).

[9] M. Hudl *et al.*, Phys. Rev. B **84**, 180404 (2011).

[10] P. Cossee and A. E. V. Arkel, J. Phys. Chem. Solids **15**, 1 (1960).

[11] J. L. Her, Y. H. Matsuda, K. Suga, K. Kindo, S. Takeyama, H. Berger, and H. D. Yang, J. Phys. Condens. Matter **21**, 436005 (2009).

[12] J. L. Her, K. Suga, K. Kindo, S. Takeyama, H. Berger, H. D. Yang, and Y. H. Matsuda, J. Low Temp. Phys. **159**, 101 (2010).

[13] J. L. Her, Y. H. Matsuda, R. Sakakura, K. Kindo, S. Takeyama, H. Berger, and H. D. Yang, J. Phys. Soc. Jpn. **79**, 085002 (2010).

[14] Y. Tokura and S. Seki, Adv. Mater. **22**, 1554 (2010).

[15] J. Coroneus, B. Alavi, and S. E. Brown, Phys. Rev. Lett. **70**, 2332 (1993).